INTERNATIONAL JOURNAL FOR NUMERICAL METHODS IN FLUIDS
Int. J. Numer. Meth. Fluids 2005; **48**:607–629
Published online 22 April 2005 in Wiley InterScience (www.interscience.wiley.com). DOI: 10.1002/fld.939

Finite volume solution of the Navier–Stokes equations in velocity–vorticity formulation

Baoshan Zhu*,†

Department of Thermal Engineering, Tsinghua University, Beijing 100084, China

SUMMARY

For the incompressible Navier–Stokes equations, vorticity-based formulations have many attractive features over primitive-variable velocity–pressure formulations. However, some features interfere with the use of the numerical methods based on the vorticity formulations, one of them being the lack of a boundary conditions on vorticity. In this paper, a novel approach is presented to solve the velocity–vorticity integro-differential formulations. The general numerical method is based on standard finite volume scheme. The velocities needed at the vertexes of each control volume are calculated by a so-called generalized Biot–Savart formula combined with a fast summation algorithm, which makes the velocity boundary conditions implicitly satisfied by maintaining the kinematic compatibility of the velocity and vorticity fields. The well-known fractional step approaches are used to solve the vorticity transport equation. The paper describes in detail how we accurately impose no normal-flow and no tangential-flow boundary conditions. We impose a no-flux boundary condition on solid objects by the introduction of a proper amount of vorticity at wall. The diffusion term in the transport equation is treated implicitly using a conservative finite update. The diffusive fluxes of vorticity into flow domain from solid boundaries are determined by an iterative process in order to satisfy the no tangential-flow boundary condition. As application examples, the impulsively started flows through a flat plate and a circular cylinder are computed using the method. The present results are compared with the analytical solution and other numerical results and show good agreement. Copyright © 2005 John Wiley & Sons, Ltd.

KEY WORDS: velocity–vorticity formulation; finite volume; integral formulae; fractional step method; vorticity boundary conditions

1. INTRODUCTION

Vorticity plays an important role in fluid dynamics analysis and in many cases it is advantageous to describe dynamics events in a flow in terms of the evolution of the vorticity

*Correspondence to: Baoshan Zhu, Department of Thermal Engineering, Tsinghua University, Beijing 100084, China.
†E-mail: bszhu@mail.tsinghua.edu.cn

Received 7 September 2002
Revised 12 August 2004
Accepted 15 December 2004

field [1]. Vorticity–velocity schemes have distinct advantages over velocity–pressure formulations for solving the Navier–Stokes equations and have become one of most interesting areas of research in computational fluid dynamics [2, 3]. All these schemes use the vorticity transport equation to determine the vorticity but they differ in the solution procedure for the velocity field from the vorticity distribution. There are two separate types of approaches in the solution procedure for the velocity field from the vorticity distribution. One is based on the differential form of the Navier–Stokes equations, solving both the continuity equation and the definition of vorticity [4, 5] or Poisson equation for the velocity based on the vorticity [6–9]. The other is the so-called integral formulation [10–13], in which an integral equation for calculating velocity explicitly from the vorticity is employed. The integral form is interesting; first, in this formulation, only non-negligible vorticity region needs to be solved. Second, it separates the velocity calculation from the vorticity redistribution, which allows an explicit, point-to-point calculation of velocity, and the velocity boundary condition at infinity is exactly satisfied. The most important point is that the integral formulation connects vorticity boundary conditions with the instantaneous vorticity and velocity distributions in the flow domain and reduces the global vorticity constraints to boundary integral equation or even a local condition.

When the integral form is used to obtain the velocity field from the vorticity field, one popular class of the methods to advance the solution of the space–time domain is the gridless Lagrangian methods, which are usually called Lagrangian vortex methods. In a vortex method, the continuous vorticity field is represented by a number of overlapping vortex particles. These particles are then tracked in a Lagrangian manner as they follow the fluid flow. A Biot–Savart law is used to get the velocity field in terms of the vorticity and vortex particles participate a random walk [12], or core-spreading [14] to simulate viscous diffusion. From a numerical point of view, the vortex methods have attractive features [14–16] and they have been mainly used to simulate the unsteady flows around the bluff bodies [17, 18]. On the other hand, there are some problems with the vortex methods. Lagrangian description of the vortex particles' movement may make the particle distribution become uneven and destroy the overlapping conditions which necessitates a remeshing process [19]. The vorticity boundary conditions are difficult to deal with although some efforts have been made [11, 20].

In this paper, an attempt is made to avoid some of the questions raised by using the gridless Lagrangian methods. The general numerical method is based on standard finite volume and finite difference techniques. Since vorticity is a conserved quantity in two dimensions, finite volume method is an appropriate scheme for vorticity transport equation while the velocity needed at the vertexes of each control volume can be calculated by using the integral form in conjunction with an adaptive fast summation algorithm. A key component of our work is to describe in detail how we accurately deal with the vorticity boundary condition along the no-slip boundary. To solve the vorticity transport equation, we split the convection term from the diffusion term using a fractional step approach. During the convection step, we impose a no-flux boundary condition on solid objects and appropriate inflow–outflow conditions on the computational domain. The diffusion term in the transport equation is treated implicitly, also using a conservative finite volume update. In each partial cell, the diffusive fluxes at partial cell edges are computed accurately using bilinear interpolation. Vorticity is diffused into the domain from solid boundaries and a no-flux condition is imposed on the computational domain. The inherent conservative property of the finite volume method guarantees the conservation of vorticity in the entire flow. It is straightforward to extend the method to 3-D flow problems, although the question of vorticity divergence remains.

The rest of the paper is organized as follows. Section 2 describes velocity–vorticity formulations of the Navier–Stokes equation for general cases, including a Poisson equation of the pressure based on velocity and vorticity. In Section 3, we present the integral form for the velocity and pressure based on the vorticity, followed by a fast summation algorithm in integral calculations. Section 4 provides a detailed description of the numerical implementation for the vorticity transport equation, especially the implementation of vorticity boundary conditions. In Section 5, numerical results are presented and analysed. Some conclusions will be given in Section 6.

2. GOVERNING EQUATIONS

The Navier–Stokes and continuity equation for the unsteady flow field with uniform density ρ and kinematic viscosity v and subject to negligible body forces are expressible in term of the velocity $\mathbf{u}$ and the pressure p as

$$\frac{\partial \mathbf{u}}{\partial t} + (\mathbf{u} \cdot \nabla)\mathbf{u} = -\frac{1}{\rho}\nabla p + v\nabla^2 \mathbf{u} \tag{1}$$

$$\nabla \cdot \mathbf{u} = 0 \tag{2}$$

Instead of solving the Navier–Stokes equations in terms of primary variables as shown in Equation (1), the vorticity-based methods usually seek the solution of the following equations:

$$\frac{\partial \boldsymbol{\omega}}{\partial t} + (\mathbf{u} \cdot \nabla)\boldsymbol{\omega} = v\nabla^2 \boldsymbol{\omega} \tag{3}$$

$$\nabla^2 \mathbf{u} = -\nabla \times \boldsymbol{\omega} \tag{4}$$

Here we assume that the flow is two-dimensional. Equation (3) is employed to determine the vorticity in the vorticity-based methods and Poisson Equation (4) is usually used to determine the velocity from the vorticity, which can be obtained by taking the curl of vorticity definition $\omega = \nabla \times \mathbf{u}$ and continuity equation $\nabla \cdot \mathbf{u} = 0$. Let the flow domain be V and with boundary S. The boundary conditions are

$$\mathbf{n} \times \mathbf{u} = \mathbf{n} \times \mathbf{u}(S), \quad \mathbf{n} \cdot \mathbf{u} = \mathbf{n} \cdot \mathbf{u}(S) \tag{5}$$

Hereafter, $\mathbf{n}$ is the unit normal vector on the boundary S pointing out of the fluid and $\mathbf{u}$ on the boundary S is usually known beforehand. The boundary may consist of a solid surface B and infinite boundary S_∞.

One advantage of the vorticity–velocity formulations over velocity–pressure formulations is its elimination of the pressure variable. After the calculation of the velocity and vorticity distribution, if necessary, we can obtain the pressure distribution according to the following Poisson equation. By taking divergence of the Navier–Stokes equation and introducing a Bernoulli-type variable H, a Poisson equation for body surface pressure can be obtained as

$$\nabla^2 H = \nabla \cdot (\mathbf{u} \times \boldsymbol{\omega}) \tag{6}$$

where

$$H = \frac{p}{\rho} + \frac{u^2}{2} \tag{7}$$

as $\mathbf{r} \to \infty$, assume $H = p/\rho + U_\infty^2/2 \to \text{const}$ (for external flow with uniform velocity at infinity).

3. INTEGRAL FORMULATIONS FOR VELOCITY AND PRESSURE

Both the Poisson Equations (4) and (6) can be solved in integral expressions in Green's function formulations. From Equation (4), the integral formulation to calculate the velocity has been derived independently by several investigators including Wu and Thompson [10], and Morino [21]. The integral presentation, which can be called generalized Biot–Savart formulation is

$$\mathbf{u}(\mathbf{r},\mathbf{t}) = \frac{1}{2\pi}\int_V \frac{\boldsymbol{\omega}(\mathbf{r}_0)\times\mathbf{R}}{R^2}\,\mathrm{d}V(\mathbf{r}_0) + \frac{1}{2\pi}\int_S \frac{[\mathbf{u}(\mathbf{r}_0)\times\mathbf{n}(\mathbf{r}_0)]\times\mathbf{R} - [\mathbf{u}(\mathbf{r}_0)\cdot\mathbf{n}(\mathbf{r}_0)]\cdot\mathbf{R}}{R^2}\,\mathrm{d}S(\mathbf{r}_0) \tag{8}$$

where $R = |\mathbf{R}| = |\mathbf{r} - \mathbf{r}_0|$, subscript '0' indicates that the variables and the integrations are performed in the $\mathbf{r}_0$ space. This equation shows that if the vorticity $\omega(\mathbf{r}_0, t)$ is known and the domain V is large enough to contain all the vorticity generated at the solid boundary prior to time t, the velocity distribution in the flow field can be evaluated directly. In Equation (8), the second integral can be reexpressed considering the uniform flow condition in infinite boundary S_∞

$$\mathbf{u}(\mathbf{r},\mathbf{t}) = \frac{1}{2\pi}\int_V \frac{\boldsymbol{\omega}(\mathbf{r}_0)\times\mathbf{R}}{R^2}\,\mathrm{d}V(\mathbf{r}_0) + \frac{1}{2\pi}\int_B \frac{[\mathbf{u}(\mathbf{r}_0)\times\mathbf{n}(\mathbf{r}_0)]\times\mathbf{R} - [\mathbf{u}(\mathbf{r}_0)\cdot\mathbf{n}(\mathbf{r}_0)]\cdot\mathbf{R}}{R^2}\,\mathrm{d}B(\mathbf{r}_0) + U_\infty \tag{9}$$

Equation (9) is valid only for certain kinematically admissible interior vorticity field, ω, and velocity boundary conditions written as Equation (5). For example, assume that Equation (9) is satisfied at a given time t, and consider an explicit time integration of vorticity equation (3). After the vorticity field has been transported but without properly taking into account the production and transport of vorticity at the boundary, Equation (9) is no longer generally satisfied; however, we can use this equation to link the vorticity existing in the flow domain with the vorticity creation on the boundary as shown in the following part.

The Green's function solution of Equation (6) is

$$\int_V H\nabla^2 G\,\mathrm{d}V + \int_H H\nabla G\cdot\mathbf{n}\,\mathrm{d}S = \int_B \nabla H\cdot\mathbf{n}G\,\mathrm{d}S + \int_V \nabla G\cdot(\mathbf{u}\times\boldsymbol{\omega})\,\mathrm{d}V \tag{10}$$

where G is $G = 1/(2\pi)\ln(1/R)$, $R = |\mathbf{R}| = |\mathbf{r} - \mathbf{r}_0|$ for two-dimensional flows. Taking the inner product of the Navier–Stokes equation with n, yields an expression of $\nabla H \cdot n$ as

$$\nabla H \cdot \mathbf{n} = \mathbf{n} \cdot \left(-\frac{\partial \mathbf{u}}{\partial t} + \mathbf{u} \cdot \boldsymbol{\omega} + \nu \nabla \times \boldsymbol{\omega} \right) \tag{11}$$

Substituting Equation (11) into Equation (10) and using the divergence theorem yields a boundary-integral equation for H as

$$\beta H + \frac{1}{2\pi} \int_B H \frac{\partial \ln(1/R)}{\partial \mathbf{n}} \, \mathrm{d}S = \frac{1}{2\pi} \int_B \frac{\partial \mathbf{u}}{\partial t} \cdot \mathbf{n} \ln(1/R) \, \mathrm{d}S - \frac{1}{2\pi} \int_B \nu \frac{\mathbf{R} \cdot (\mathbf{n} \times \boldsymbol{\omega})}{R^2} \, \mathrm{d}S - \frac{1}{2\pi} \int_V \frac{\mathbf{R} \cdot (\mathbf{u} \times \boldsymbol{\omega})}{R^2} \, \mathrm{d}V \tag{12}$$

where β is $\beta = 1$ inside the flow field and $\beta = \frac{1}{2}$ on the boundary B. When the surface pressure is computed according to Equation (12), the left-hand side of the equation represents a matrix formulation which must be decomposed on the first time when there is no relative movement among the flow boundaries. The right-hand side accounts for the motion of the bodies and the volume vorticity in the flow field.

The integral representations (9) and (12) permit the explicit, point to point, computation of the new velocity and pressure distribution, and only the non-zero vorticity region needs to be solved. It is easy to check if the integral formula would incur a heavy computation cost; a calculation of $O(N_v^2)$ interaction is necessary for N_v control volumes with non-zero vorticity. However, note from Equations (9) and (12) that both the velocity and pressure induced by a control volume drop off as the inverse of distance in the far field motivates methods to approximate (9) and (12) by grouping the influence of distant vortex volumes to reduce computational cost. These approximations are crucial in making the integral computations of challenging problems practically feasible.

By assuming that the vorticity has a uniform distribution within each control volume, the velocity at a point $\mathbf{r}_j$ induced by vorticity distribution in the flow domain, in particular at the vertexes of each control volume is given by

$$\mathbf{u}_j(\mathbf{r}_j, t) = \frac{1}{2\pi} \sum_{i=1}^{N_v} \frac{\omega_i(t)\mathbf{k} \times (\mathbf{r}_j - \mathbf{r}_i)}{|\mathbf{r}_j - \mathbf{r}_i|^2} \mathrm{d}V_i \tag{13}$$

In this study, an approach by Barnes and Hut [22] has been modified to reduce the computational cost to $O(N_v \log N_v)$ by grouping the influence of distant computational elements and utilizing a Laurent expansion in (13). In this analysis, the point vortex representation is assumed for the vorticity volume. This is a reasonable assumption since the effect of volume shape becomes negligible for distant elements. Consider a complex variable representation of (13) for a group of point vortices given by

$$u(Z) = \frac{i}{2\pi} \sum_{n=1}^{M} \frac{\Gamma_n}{Z - Z_n} \tag{14}$$

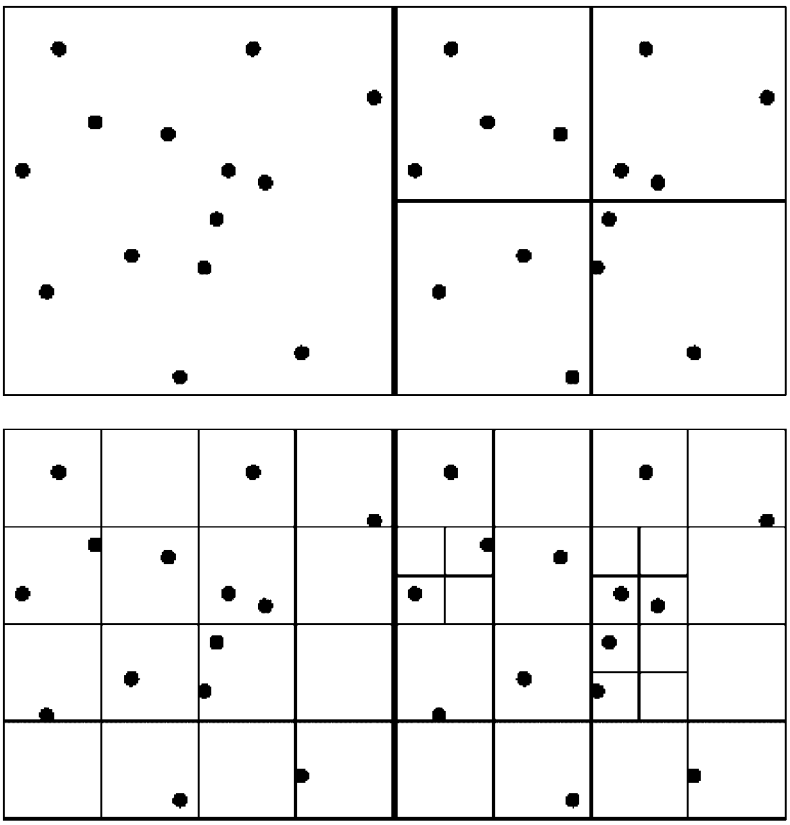

Figure 1. Hierarchical zone structure.

in which, a point vortex at the centre, $\mathbf{r}_n$, of a control volume Ω_n of area A_{Ω_n} with the strength of $\Gamma_n = \omega_n A_{\Omega_n}$. Introduce a new location Z_m that will serve as a point about which to expand the influence of groups of far field particles

$$u(Z) = \frac{i}{2\pi} \frac{1}{Z - Z_m} \sum_{k=0}^{p} \frac{\alpha_k}{(Z - Z_m)^k} + O\left(\left| \frac{Z_m - Z_n}{Z - Z_m} \right|^{p+1} \right) \tag{15}$$

where $\alpha_k = \sum_{n=1}^{M} \Gamma_n (Z_m - Z_n)^k$, and $|z - z_m| \gg |z_n - z_m|$. In actual calculation, the distance between z and z_m is greater than some factor times the radius λ of the zone [22].

The summation over M particle can be thus reduced to a summation over $P + 1$ terms involving coefficients α_k that can be precomputed and perused for each summation over the group of particles. The error term defines the need for the particle group to reside in the far field of the point Z.

Similar formula transformation can also be done for the term $(1/2\pi) \int_V [\mathbf{R} \cdot (\mathbf{u} \times \boldsymbol{\omega})]/R^2$ in the pressure integral equation. An entire hierarchy of grouping has been developed with a quad-tree structure to allow for maximal use of the above approximations. An hierarchical example is provided in Figure 1. The whole flow domain containing non-zero vorticity is

initially contained in a single square zone. This is then divided into four subzones. Each zone is then further subdivided into four new zones, provided that there is a minimum number of particles in the zero, thus creating a hierarchical structure of zones. For each zone, the parent zone and any children of the zero are recorded, along with which particles are stored in that zone.

4. SOLUTION OF VORTICITY TRANSPORT EQUATION

Since vorticity is a conserved quantity in two dimensions, finite volume method is an appropriate scheme for vorticity transport equation. Using the cell-centred finite volume method, for each control volume (i, j), see Figure 2, the vorticity transport equation (3) can be written in the integral form as

$$\frac{\partial}{\partial t}\int_{V_c} \omega \, \mathrm{d}V + \int_{S_c} (\mathbf{u}\cdot\mathbf{n})\omega \, \mathrm{d}S = \nu \int_{S_c} \nabla\omega \cdot \mathbf{n} \tag{16}$$

where $\mathbf{n}$ is the unit normal vector of the control surface S_c and for simplicity, the orthogonal grids have been used to discretize the flow domain, and $\Delta\eta$ and $\Delta\xi$ are the measures of edges. For diffusive fluxes, a simple linear interpolation can be used for calculating the gradient for an orthogonal co-ordinate system which is the case of the present study. If more general cases with non-orthogonal co-ordinate system are involved, the method involving the transformation of the derivative into a surface integral using the Gauss theorem can be employed.

The main challenge in solving Equation (16) is to impose the no-slip boundary condition. It is clear that it is possible to derive proper velocity boundary conditions for the Navier–Stokes equations. In primitive variable (u–p) formulation of the Navier–Stokes equations, the no-slip boundary condition is explicitly enforced. The no-slip condition physically means the creation of vorticity at the boundary. In vorticity–velocity formulations, vorticity conditions are required for formulating and quantifying this vorticity creation process. In general, involving the vorticity creation on the boundary, two different schemes are usually referred, one is the boundary value of vorticity (Dirichlet-type boundary condition) the other is the wall-normal vorticity flux (Neumann-type boundary condition). The Neumann form of the boundary condition is, in general, preferred. For Neumann-type vorticity condition, the task is to derive the vorticity flux at the boundary. In this section, we implement the boundary conditions in a fractional step algorithm, which formulates the problem as a succession of inviscid and viscous subjects. The convection and diffusion are combined using a standard fractional step approach.

4.1. The convection equation

Let us assume that in the nth time step an admissible vorticity field has been computed and we seek to advance the solution of the next step. For the convective operator, we solve

$$\frac{\partial}{\partial t}\int_{V_c} \omega \, \mathrm{d}V + \int_{S_c} (\mathbf{u}\cdot\mathbf{n})\omega \, \mathrm{d}S = 0 \tag{17}$$

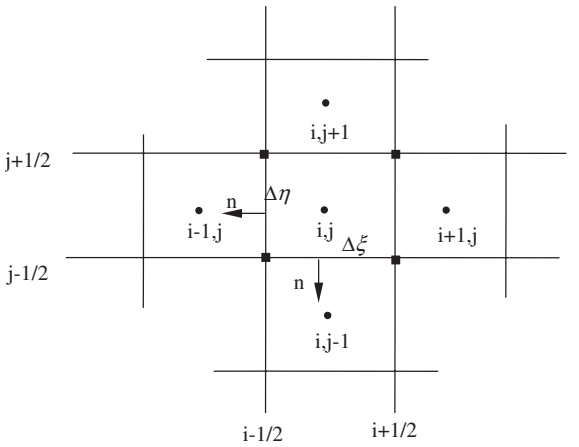

Figure 2. Schematic of orthogonal control volume.

The second-order Adams–Bathforth method has been used to advance the solution in the time domain.

Let $D_{i-1/2,j}$ and $E_{i,j-1/2}$ represent the convection flux at the left edge and bottom edge for cell (i,j) shown in Figure 2. The convective flux-term for each of the cell faces in (17) is easily computed

$$D_{i-1/2,j} = \frac{\mathbf{u}_{i-1/2,j-1/2} + \mathbf{u}_{i-1/2,j+1/2}}{2} \cdot \mathbf{n}_{i-1/2,j}\omega_{i,j} \tag{18}$$

$$E_{i,j-1/2} = \frac{\mathbf{u}_{i-1/2,j-1/2} + \mathbf{u}_{i+1/2,j-1/2}}{2} \cdot \mathbf{n}_{i,j-1/2}\omega_{i,j} \tag{19}$$

Note that the convective velocity $(\mathbf{u} \cdot \mathbf{n})$ (assumed to be positive) convects vorticity assigned to the upwind node. If $(\mathbf{u} \cdot \mathbf{n})$ turns to be negative, then the vorticity is assigned the value $\omega_{i-1,j}$ in (18), $\omega_{i,j-1}$ in (19).

After the vorticity has been convected but without properly taking into account the production and transport at the boundary, Equation (9) is no longer generally satisfied. As proposed by Lighthill [23], we represent the circulation associated with the newly created vorticity by a vortex sheet to reestablish kinematic compatibility. Conveniently enough, the boundary integrals in Equation (9) represent the notion induced by vortex sheets and source sheets with strength γ and σ, respectively, given by

$$\gamma = -\mathbf{n} \times \mathbf{u}, \quad \sigma = -\mathbf{n} \cdot \mathbf{u} \tag{20}$$

A convenient method of the solving the vortex sheet is to solve the integral equation on the condition $\sigma = 0$, i.e. satisfying the no-flux boundary condition

$$\frac{1}{2\pi}\int_B \frac{\gamma(\mathbf{r}_0)\times\mathbf{R}}{R^2}\,\mathrm{d}B(\mathbf{r}_0) = -\frac{1}{2\pi}\int_V \frac{\omega(\mathbf{r}_0)\times\mathbf{R}}{R^2}\,\mathrm{d}V(\mathbf{r}_0) - U_\infty \tag{21}$$

We obtain a unique solution for this equation by adding a constraint on the strength of the vortex sheet. Similarly, to get Equation (11), we can derive a relation for the tangential derivative of H in the solid boundary B

$$\frac{\partial H}{\partial \tau} = \frac{\partial \gamma}{\partial t} + \nu\frac{\partial \omega}{\partial \mathbf{n}} \tag{22}$$

For physical reasons we shall impose that H be continuous over the solid. By integration, Equation (22) leads to

$$\frac{\mathrm{d}}{\mathrm{d}t}\int_B \gamma\,\mathrm{d}s + \nu\int_B \frac{\partial \omega}{\partial \mathbf{n}} = 0 \tag{23}$$

On the other hand, after some simple transformations, integration of the vorticity transport Equation (3) over the domain V gives

$$\frac{\mathrm{d}}{\mathrm{d}t}\int_V \omega\,\mathrm{d}V = \nu\int_B \frac{\partial \omega}{\partial n}\,\mathrm{d}B \tag{24}$$

This shows that when there is no convection flux through the domain boundary, the only way that vorticity can enter is by diffusion from the solid surface. From Equations (23) and (24), via integration in time, we obtain

$$\int_V \omega\,\mathrm{d}V + \int_B \gamma\,\mathrm{d}B = \text{const} \tag{25}$$

The solution of Equation (21) yields the vortex sheet strength γ, representing the creation of vorticity during a given time step. We may think of the vortex sheet γ as part of the interior vorticity. On the fluid side of the sheet, the tangential velocity is determined from the vorticity within the domain and the velocity boundary condition, while on the nofluid side, the velocity is specified by the boundary condition. Across the vortex sheet, there is a jump in tangential velocity equal to the strength of the sheet. The effects of the diffusion step described in following are in particular immediate regularization of the discontinuous velocity profile, establishing a proper boundary layer.

4.2. The diffusion equation

For the diffusion, we wish to solve numerically

$$\frac{\partial}{\partial t}\int_{V_c} \omega\,\mathrm{d}V = \nu\int_{S_c} \nabla\omega\cdot\mathbf{n}\,\mathrm{d}S \tag{26}$$

This equation shows that the vorticity for each cell is updated in each time step by approximations to the flux through each edge of cell. Let $F_{i-1/2,j}$ and $G_{i,j-1/2}$ represent the diffusion flux at left edge and bottom edge shown in Figure 1. We approximate quantities $F_{i-1/2,j}$ and

$G_{i,j-1/2}$ on orthogonal cell edges by differencing across the edges and use these to approximate the diffusion fluxes as

$$F_{i-1/2,j} = -\nu \frac{\omega_{i,j} - \omega_{i-1,j}}{\xi_{i,j} - \xi_{i-1,j}} \tag{27}$$

$$G_{i,j-1/2} = -\nu \frac{\omega_{i,j} - \omega_{i,j-1}}{\eta_{i,j} - \eta_{i-1,j}} \tag{28}$$

To discretize the diffusion equation (26), we use a standard Crank–Nicolson method at all grid points. We define an approximation to the integral $\nu \int_S \nabla\omega \cdot n \, \mathrm{d}S$ in Equation (26) as

$$W_{ij}^n = -[\Delta\eta(F_{i+1/2,j}^n - F_{i-1/2,j}^n) + \Delta\xi(G_{i,j+1/2}^n - G_{i,j-1/2}^n)] \tag{29}$$

Then an implicit discretization of Equation (26) is given by

$$\Delta\xi\Delta\eta \frac{w_{ij}^{n+1} - \omega_{ij}^n}{\Delta t} = \frac{1}{2}(W_{ij}^n + W_{ij}^{n+1}) \tag{30}$$

We use the Peaceman–Rachford ADI scheme to solve this equation. Thus the resulting system of equations are tridiagonal. To close the equations, we need to know vorticity flux $(\partial\omega/\partial\mathbf{n})_B$ on the solid boundary. Similar with Kinney and Paolino [11], and Koumoutsakos *et al.* [20], we envision the vortex sheet as equivalent to the vorticity flux. The vorticity flux helps establish a vorticity field that eliminates the spurious tangential velocity while simultaneously enforcing the no-flux boundary condition. Here we should notice that the vorticity flux $\nu(\partial\omega/\partial\mathbf{n})_B$ is coupled globally to vorticity distribution in flow domain according to Equations (8) and (25). We introduce an iterative scheme to solve this coupled system [24]. Let $\sigma = \nu(\partial\omega/\partial\mathbf{n})|_B$, we may obtain a first-order formulation for σ from Equation (25) as

$$\sigma = -\frac{\gamma}{\Delta t}\bigg|_B = \frac{u_\tau}{\Delta t}\bigg|_B \tag{31}$$

An iterative scheme can be naturally derived from (31). For nth time step, after convection, the spurious tangential velocity $u_\tau^{n+1/2}$ occur on the solid boundary, therefore

$$\sigma = \frac{\mathbf{u}_\tau^{n+1/2}}{\Delta t}\bigg|_B \tag{32}$$

For a fully decoupled scheme, Equation (32) is the boundary condition to use. After the diffusion, $\mathbf{u}_\tau^{n+1}$ in general not zero, $\mathbf{u}_\tau^{n+1} \neq 0$. Therefore, utilizing (32) to determine the vorticity flux from the solid boundary introduces some error into the solution and the no-slip condition is not strictly satisfied. Although the error is generally not large, as an unknown factor, it is undesirable for designing highly accurate numerical schemes. Thus, we introduce an iterative method to control the slip to a desired small level. In this iterative scheme, an update vorticity flux is used as

$$\sigma^{m+1} = \sigma^m + \frac{u_\tau^{n+1,m}}{\Delta t} \tag{33}$$

where m is the number of iterative times. Clearly, (33) converges as the no-slip condition is achieved. Note that during iteration only the slip velocity needs to be computed. This

feature makes (33) fit well in this integral method that solves velocity via the generalized Biot–Savart integration, because the slip velocity can be obtained without solving the whole velocity field.

4.3. Fractional step methods for the vorticity transport equation

In the previous two Sections 4.1 and 4.2, we have described in detail our algorithms for handling the convection and diffusion terms separately. These can be combined using standard fractional step methods in order to solve the coupled convection–diffusion equation. The advantage of using a fractional step approach is that we can treat the vorticity convection, creation and diffusion separately.

In the fractional step approach, both the first-order scheme (Godunov splitting) and the second-order scheme were considered,

$$\omega(n\Delta t) = (E(\Delta t)H(\Delta t))^n \omega_0 \quad \text{(Godunov splitting)} \tag{34}$$

$$\omega(n\Delta t) = (E(\Delta t/2)H(\Delta t)E(\Delta t/2))^n \omega_0 \quad \text{(Strang splitting)} \tag{35}$$

where $E(\Delta t)$ is the convection operator and $H(\Delta t)$ is the diffusion operator. In the Strang splitting, the half time step of convection is followed immediately (in the next step) by another half time step using the same operator. These two half steps can be combined into a single step of length Δt and in fact it is better to do so to reduce numerical diffusion and computational cost. Once this is done, the Strang splitting (35) over many time steps is identical to the Godunov splitting (34) except in the first step only at the beginning. For this reason, we use the simpler Godunov splitting, so the semi-discrete equations that we solve have the basic form

$$\frac{\omega^* - \omega^n}{\Delta t} = -(\mathbf{u} \cdot \nabla)\omega^n \tag{36}$$

$$\frac{\omega^{n+1} - \omega^*}{\Delta t} = \nu \nabla^2 \left(\frac{\omega^* + \omega^{n+1}}{2} \right) \tag{37}$$

In this method, as expressed in (36) and (37), the convection and diffusion are performed in turns and the diffusion scheme is unconditionally stable.

5. NUMERICAL RESULTS

In this section, we demonstrate the performance of our proposed algorithm through the numerical examples. One computational cycle of the present algorithm as it applies to flow simulations consists of the following steps. We assume that $\mathbf{u}_i^n$ and ω_i^n are known for N vortex cells covering the flow domain at time $n\Delta t$:

(1) Solve the convection equation (17) with $\mathbf{n} \cdot \mathbf{u} = \mathbf{0}$ on the solid boundary, satisfying the no-flux boundary condition.

(2) Use Equation (21) to determine the strengths of vorticity sheets on the boundary.
(3) Solve Equation (30) with Neumann boundary condition. Use an iterative scheme to assure the slip velocity within an acceptable minimum value.
(4) Calculate the velocity at the vertexes of vortex cells at $(n+1)$th time step using formulation (9) combined with (15).
(5) If necessary, calculate pressure distribution with Equation (12).
(6) Repeat to step 1.

Two calculated examples are given in the following in order to show the accuracy and efficiency of the proposed method. The first example is the simulation of Blasius boundary layer. The Blasius boundary was computed by time marching to a steady state after impulsively moving the fluid in an initially zero vorticity fluid. The second example is the flow around the impulsively started circular cylinder. This flow problem has been extensively used as a prototype of unsteady separated flows and a number of numerical and experimental results are available for validating new numerical methods.

5.1. The Blasius boundary layer

We calculated the Blasius boundary layer by impulsively moving the fluid around the flat plate. For this boundary layer flow, lengths are assumed to be scaled by a streamwise length of the plate, L, and velocities by the free stream velocity, U_∞. The Reynolds number $Re = U_\infty L/v$, and calculations are performed in non-dimensional flow domain $0 \leqslant x \leqslant x^*,\ 0 \leqslant y \leqslant y^*$. x^* is decided to assure the existence of contributions from vorticity lying beyond flat plane length. y^* is chosen to be large enough to contain the complete lateral boundary layer growth through flat plane length. We calculated the Blasius boundary for $Re = 10\,000$, therefore, we selected $x^* = 5.0$ and $y^* = 0.1$.

To examine the performance (timing, accuracy, etc.) of the fast summation algorithm, calculations using both the direct summation and fast algorithm are performed. A simple uniform grid is utilized for the calculation and the grid points used are 200×50. The width and height of the cells are assigned common constant values of Δx and Δy, respectively, as shown in Figure 3. The time step adopted for the calculation is $\Delta t = 0.005$ and 2000 steps have been advanced. By the last step ($t = 10$), the number of active cell, i.e. the cells with a vorticity value not less than a specified value $\omega = 10^{-6}$, is about 7800, and the CPU time used for the direct calculation is nearly four times of the fast algorithm. The number of the terms used for calculating the Laurent series expansion is $N_t = 12$. The results of vorticity from both calculations are shown in Figure 4 for the points of $x = 0.25$, 0.5 and 0.75 on the flat plate surface. No noticeable discrepancy occurs, which indicates the high accuracy

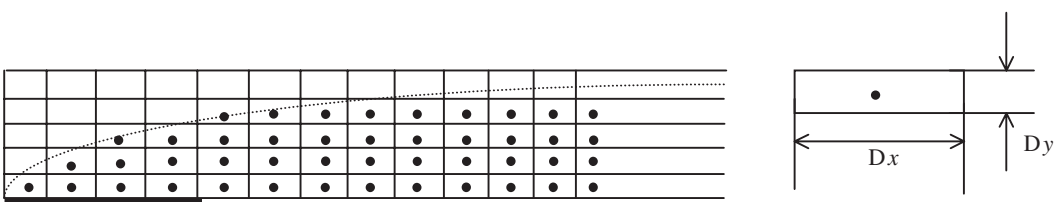

Figure 3. Schematic of vortex volume for boundary layer calculation.

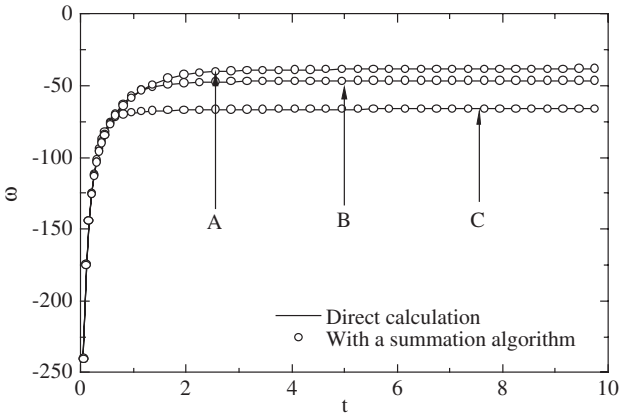

Figure 4. Accuracy of fast algorithm: vorticity for three different points at the flat plate A$(0.25, 0.0)$, B$(0.50, 0.0)$ and C$(0.75, 0.0)$ (Grid: $200 \times 50, \mathrm{d}t = 0.005$).

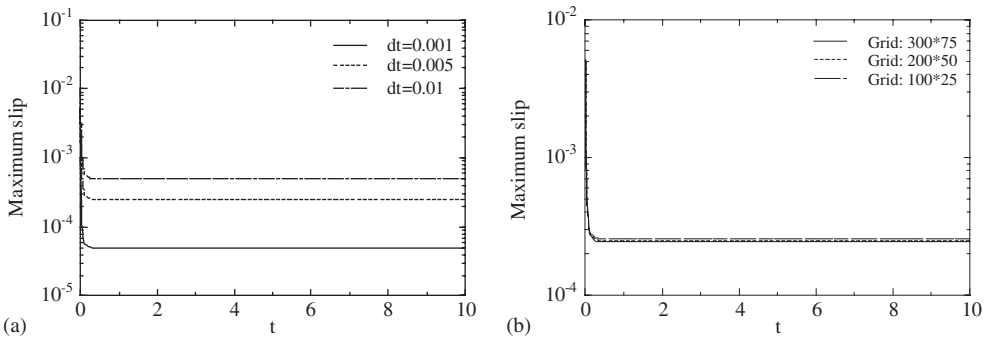

Figure 5. Effects of grid density and time step on the slip: (a) Effects of time step (Grid: 200×50): and (b) effects of grid density ($\mathrm{d}t = 0.005$).

of the fast algorithm. No examination has been made to optimize the fast algorithm during the calculation because we want to keep the same accuracy of the fast algorithm with the direct calculation. In the following discussion, all the results are obtained by using the fast summation algorithm.

In order to evaluate the influence of the grid density and time step on the solution, grid density 100×25, 200×50 and 300×75 for different non-dimensional time step $\Delta t = 0.001,\ 0.005$ and 0.01 have been used for the calculation. The time variation of the maximum slip without iteration is shown in Figure 5. Figure 5(a) shows the results for different time steps $\Delta t = 0.001,\ 0.005$ and 0.01 with grid density 200×50, and Figure 5(b) shows the results for different grid density 100×25, 200×50 and 300×75 with a fixed time step $\Delta t = 0.005$. It clearly indicates that residual slip after the diffusion substep is proportional to Δt, and the magnitude of the slip has little dependence on the grid size. Figure 5 also shows that the local and decoupled formula (31) is well applicable for the flow without iteration.

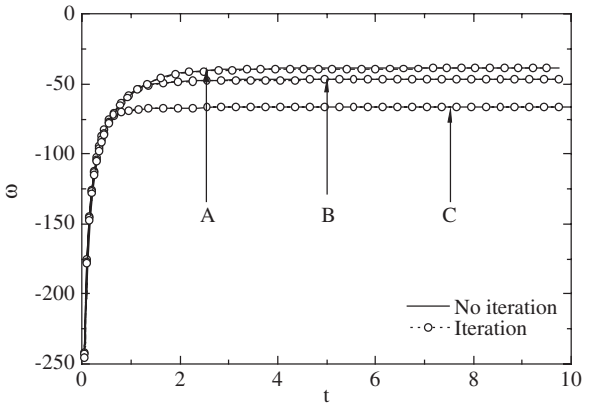

Figure 6. Effects of iteration: vorticity for the same three points A, B and C in Figure 4.

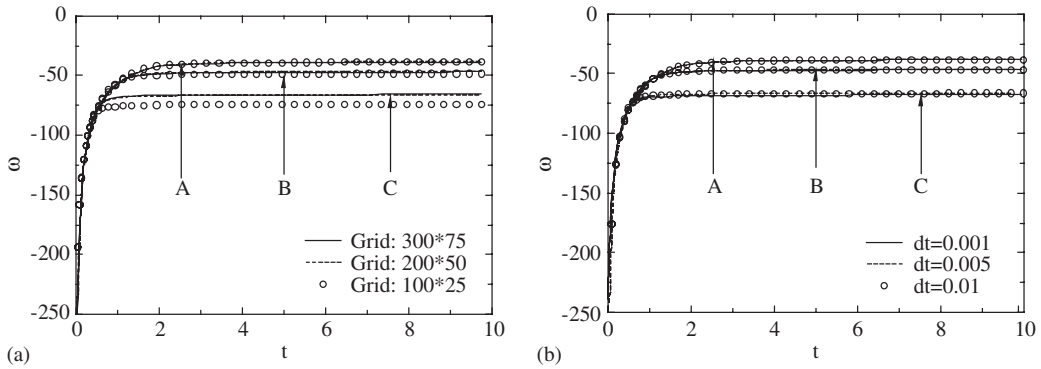

Figure 7. Vorticity variation with time for the same three points A, B and C in Figure 4: (a) Different grid density (Time step: $dt = 0.005$); and (b) different time step (Grid: 200×50).

As described in Section 4.2, we implemented the iterative scheme so that the slip could be further reduced and the global coupling was better satisfied. In the calculation, the maximum slip was reduced to below 10^{-5} and about two or three iterations were needed for convergence. The result (Figure 6) is almost identical with the non-iterative one. We want to point out that ω_B is the space-integrated effect of σ and the slip does not directly relate to the accuracy of ω_B, although vorticity is created by no-slip condition.

Figure 7 shows the results of vorticity for the points at $x = 0.25,\ 0.5$ and 0.75 on the flat plate surface with grid density $100 \times 25,\ 200 \times 50$ and 300×75 for different time steps $\Delta t = 0.001,\ 0.005$ and 0.01. Figure 7(a) shows the results with grid density $100 \times 25,\ 200 \times 50$ and 300×75, and a fixed non-dimensional time step $\Delta t = 0.005$. Figure 7(b) shows the results for different time step $\Delta t = 0.001,\ 0.005$ and 0.01 with grid density 200×50. The grid resolution study shows that the two finest grids produce nearly the same results. It is also found that the influence of Δt turns out to be small. It seems that the time accuracy is not crucial in the present early-stage computation. In summary, Figure 7 shows that the steady state can be achieved after $t \approx 4.0$ by impulsively moving the fluid around the flat plate.

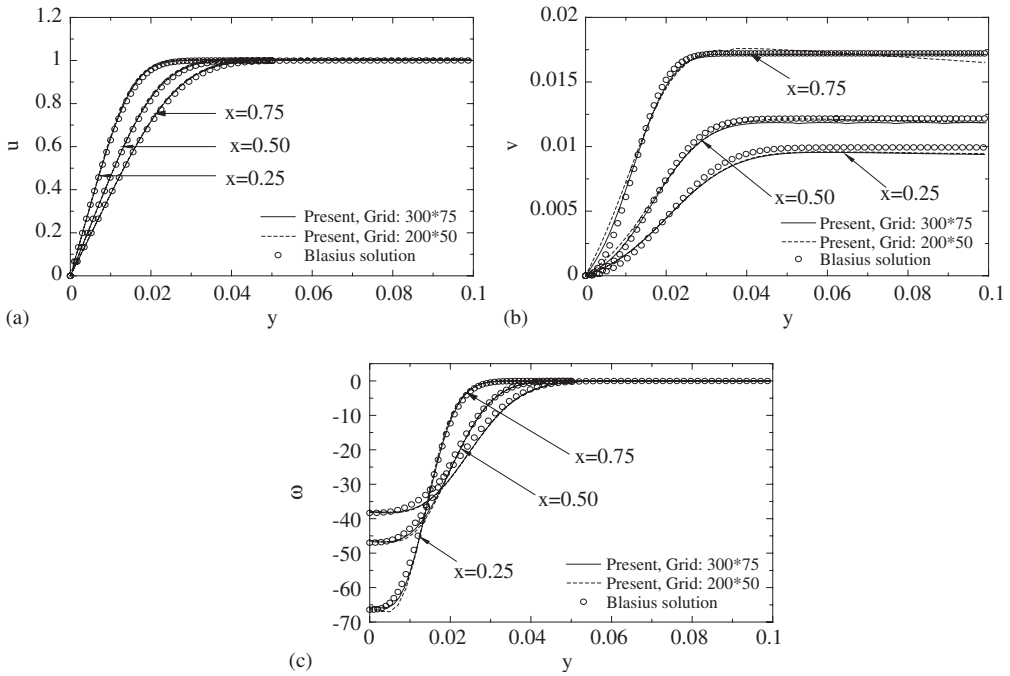

Figure 8. Velocity and vorticity predictions in the cross flow sections: $x = 0.25,\ 0.50$ and 0.75 ($\mathrm{d}t = 0.005$): (a) Streamwise velocity u; (b) cross velocity v; and (c) vorticity ω.

The solution was compared with Blasius solution. The velocity and vorticity on the cross sections through the boundary layer at $x = 0.25,\ 0.5$ and 0.75 are shown in Figure 8. The streamwise velocity agrees well with the Blasius profile. It is difficult to accurately predict the crossflow velocity v due to its very small magnitude. Although the relative errors are somewhat greater than that in the case of streamwise velocity u, the predictions of crossflow v are well credible. Figure 8(c) shows the prediction of vorticity, and vorticity ω is closely predicted including the zone near the plate wall.

The velocity and vorticity at streamwise sections $y = 0.005,\ 0.01$ and 0.02 are shown in Figure 9. Similar as on the cross-sections, both the velocity and vorticity are well predicted and agree well with the Blasius profile. Near the leading edge, the variation of crossflow velocity v and vorticity ω is significant. It should be pointed that the Blasius similarity solution predicts that v and ω are singular at $x = 0$. However, according to Figure 9, the numerical solution does not mimic the singularity in the Blasius solution. With refined resolution, the prediction of crossflow velocity v is somewhat improved, which means that the singular behaviour of the leading edge flows is partly responsible for the disparities in crossflow velocity and vorticity prediction.

Figure 10 shows the wall vorticity distribution along the flat plate. Wall vorticity distribution is well predicted and agrees well with the Blasius solution except at the leading edge. As mentioned before, vorticity ω is singular at leading edge $x = 0$. For bounded flow problems,

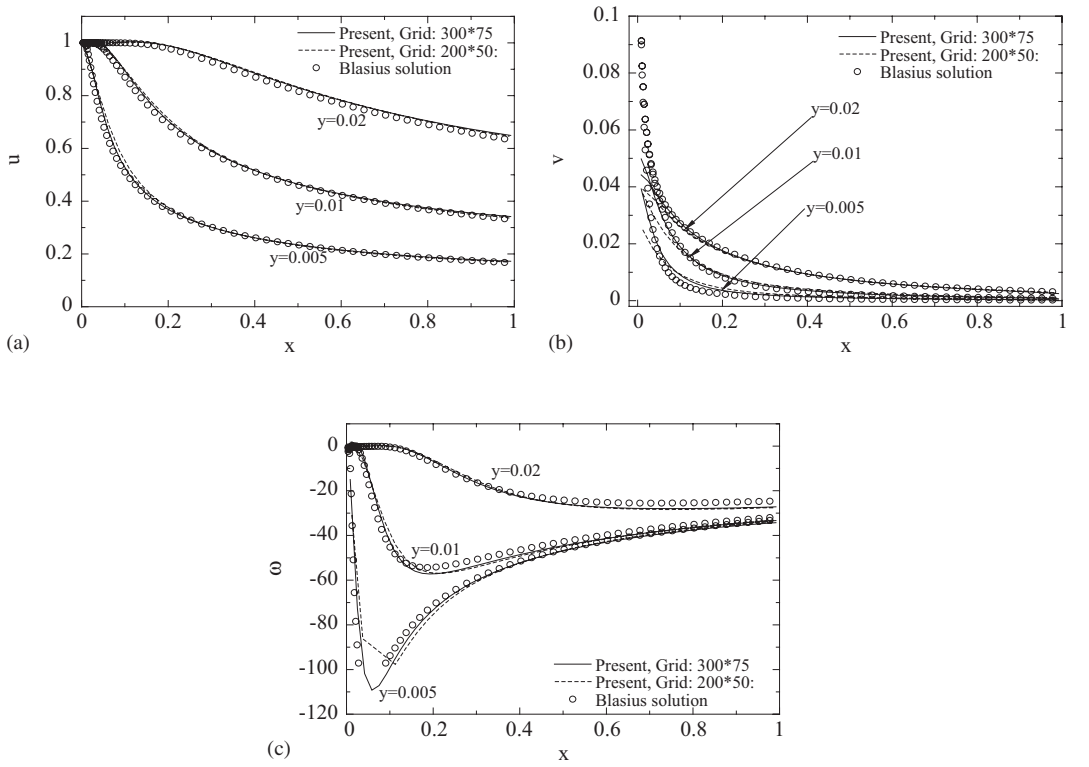

Figure 9. Velocity and vorticity predictions in the streamwise sections: $y = 0.005$, 0.01, and 0.02 ($dt = 0.005$): (a) Streamwise velocity u; (b) crossflow velocity v; and (c) vorticity ω.

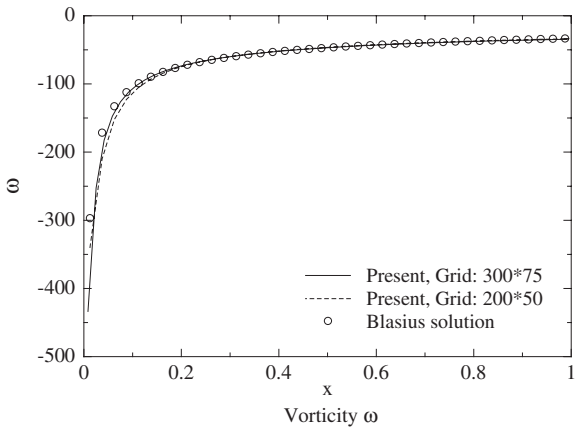

Figure 10. Vorticity prediction along the flat plate boundary $y = 0.0$ ($dt = 0.005$).

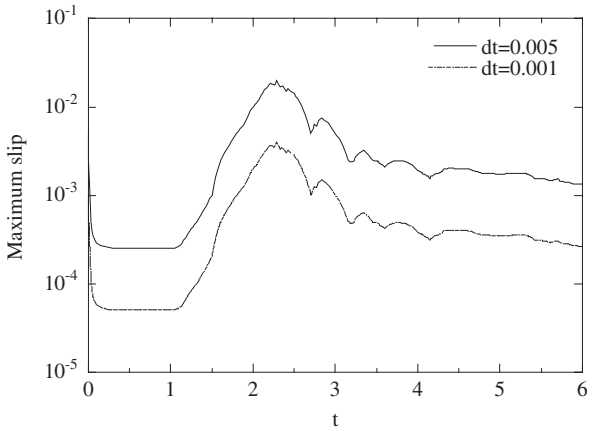

Figure 11. Time variation of maximum slip velocities for a circular cylinder: $Re = 3000$ (grid: 300×200).

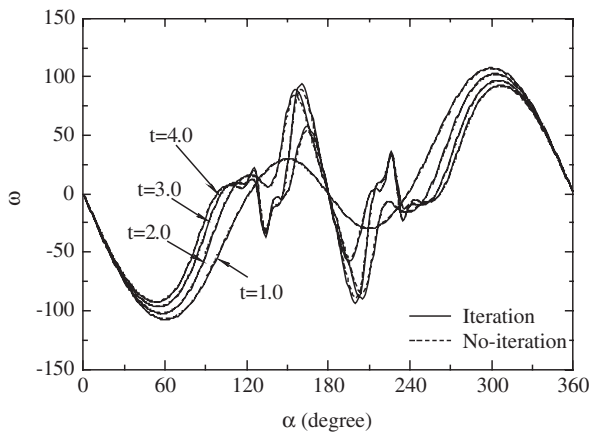

Figure 12. Surface vorticity distribution: $Re = 3000$ (grid: $300 \times 200, \mathrm{d}t = 0.005$).

there are no boundary conditions on the vorticity, but the value of the vorticity on the boundary does play a major role in most vorticity-based methods. Although flow around a flat plate is one of the simplest bounded flows, the previous results show that the present schemes are suited to compute the vorticity which is a challenging variable in vorticity-based methods.

5.2. *Flow around impulsively started circular cylinders*

To show the accuracy and efficiency of the proposed method, calculations are also performed for flows around an impulsively started circular cylinder at $Re = UD/v = 3000,\ 9500$, where U, D and v denote a uniform velocity, a diameter of the circular cylinder and the kinematic

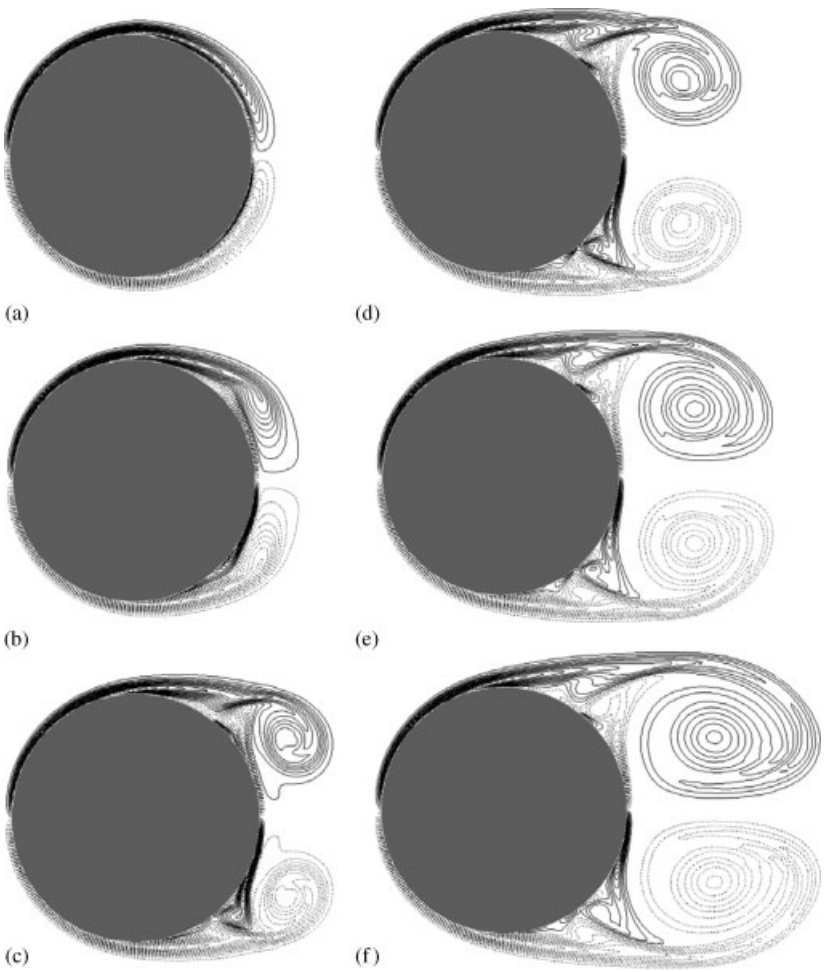

Figure 13. Instantaneous equi-vorticity contours: $Re = 3000$ (grid: $300 \times 200, \mathrm{d}t = 0.005$): (a) $t = 1.0$; (b) $t = 2.0$; (c) $t = 3.0$; (d) $t = 4.0$; (e) $t = 5.0$; and (f) $t = 6.0$.

viscosity, respectively. For both the Reynolds number, series of new separation phenomena appear which make them particularly challenging for various numerical schemes [17, 25, 26].

For $Re = 3000$, at first 300×200 grid was used with a minimum grid size in the normal direction to the surface $\Delta r = 0.01$ and the time step $\Delta t = 0.001,\ 0.005$. The time variation of the maximum with no-iteration is shown in Figure 11. It is interesting to note that after keeping at a constant level for some time, the slip rises. The time of slip rising is about the time when the first secondary vortex starts to form as shown in Figure 12. Owing to small vortices rather than the primary large vortex, the boundary vorticity no longer varies smoothly along the surface and a large gradient occurs. The small vortices can also be seen clearly in Figure 13. Comparing Figure 11 with Figure 12 shows that when $t = 2.0$, there are high peaks in the ω_B distribution, so that not only ω_B but also its gradient is large. Correspondingly, the slip is large, about the maximum point in the curve.

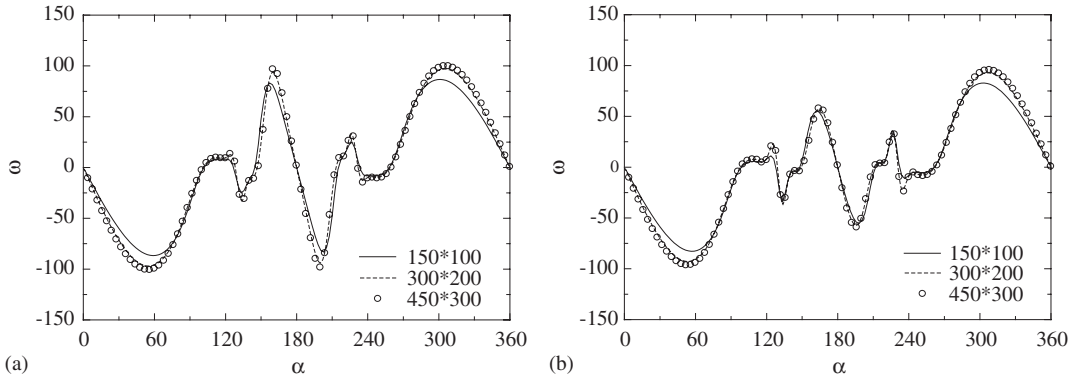

Figure 14. Surface vorticity distribution for different grid density: $Re = 3000$: (a) $t = 3.0$; and (b) $t = 4.0$.

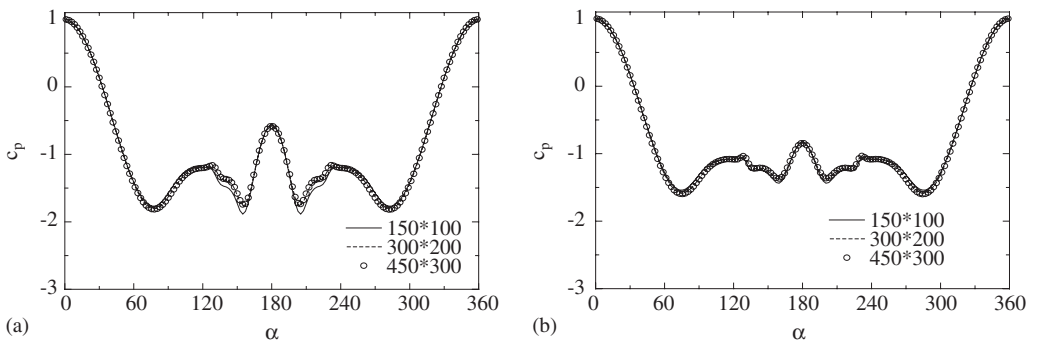

Figure 15. Surface pressure distribution for different grid density: $Re = 3000$: (a) $t = 3.0$; and (b) $t = 4.0$.

We also implemented the iterative scheme so that the slip could be further reduced and the global coupling was satisfied better. In the calculation, the maximum slip was reduced to below 10^{-5} and five to eight iterations were needed for convergence. The fast convergence of the iterative schemes is mainly because of the weak coupling of vorticity with pressure. The result (Figure 12) is almost identical with the non-iterative one.

As shown in Figure 12, there is a high peak in ω_B, the normal gradient near the wall is likely to be very high. Thus reducing Δr near the wall will give a better solution. Results of a higher grid resolution 450×300 with $\Delta r = 0.005$ and a coarser grid resolution 150×100 with $\Delta r = 0.02$ are also presented. Figure 14 shows the vorticity distribution at the body surface for $t = 3.0$ and 4.0 for different grid densities. Comparing with coarser grid density 150×100, the improvement in the peak values of boundary vorticity ω_B is obvious. Figure 15 shows the pressure distribution on the boundary surface corresponding to Figure 14. In pressure distribution, a little difference occurs at the positions with peak values of ω_B between the finer grid densities 450×300, 300×200 and the coarser grid density 150×100. The improvement

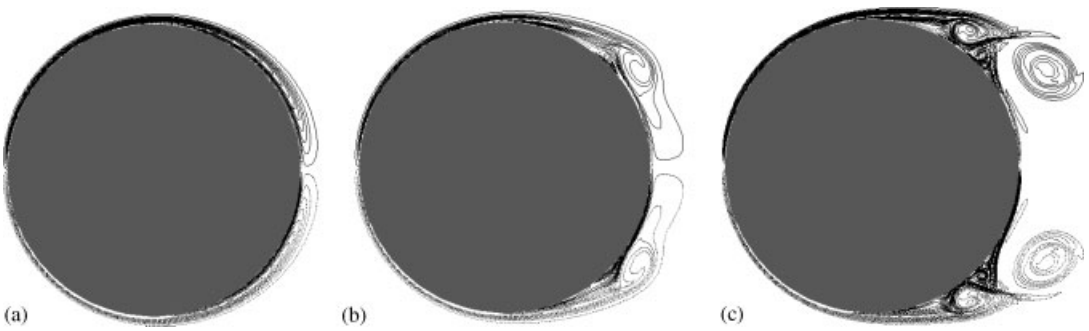

Figure 16. Instantaneous equi-vorticity contours: $Re = 9500$: (a) $t = 1.0$; (b) $t = 2.0$; and (c) $t = 3.0$.

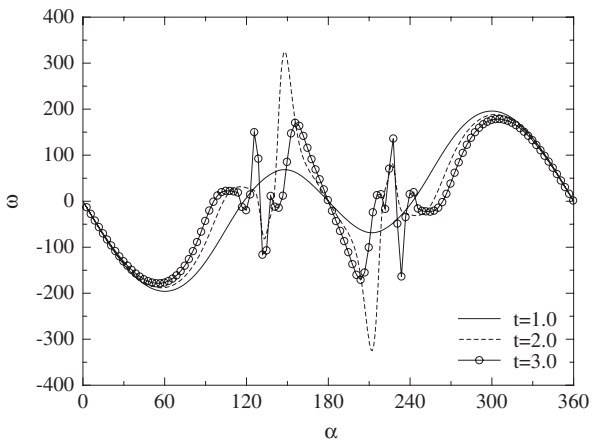

Figure 17. Surface vorticity distribution: $Re = 9500$.

in pressure distribution is less than that in vorticity distribution for finer grids. This also shows that if the vorticity has certain accuracy, the pressure will be very accurate because of its one order higher accuracy than vorticity's.

As Reynolds number Re increases from 3000 to 9500, the flow exhibits a much richer vortex structure, which makes the computation more difficult [18]. In the following results, a 600×300 grid was used with a minimum grid size in the normal direction to the surface $\Delta r = 0.005$ and the time step $\Delta t = 0.002$. It should be pointed out that although large grid points were embedded in the flow domain, the number of actually active vortex cells used in the calculation was around 35 000 by the end of the calculation $t = 3.0$.

Figure 16 shows the equi-vorticity around the cylinder and Figures 17 and 18 show the vorticity distribution and pressure distribution on the cylinder surface for $t = 1.0,\ 2.0$, and 3.0, respectively. The present calculation accurately resolved the near wall vorticity for this high Reynolds number Re, therefore, the formulation and eruption of the secondary vorticity are

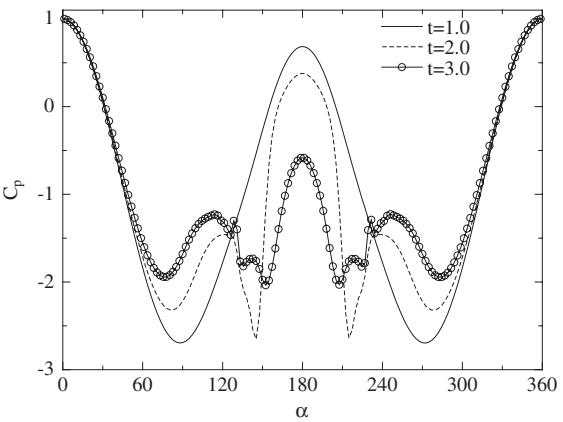

Figure 18. Surface pressure distribution: $Re = 9500$.

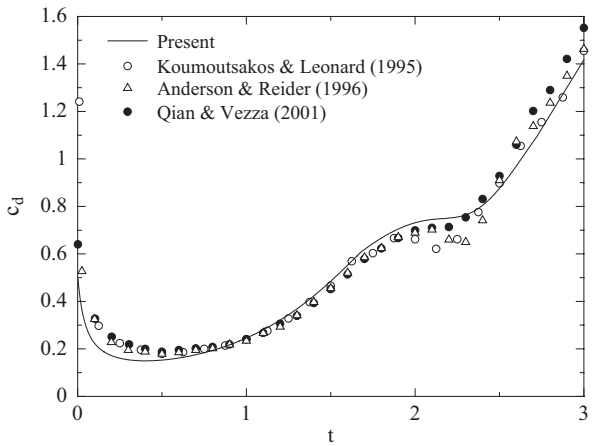

Figure 19. Comparison of drag coefficients: $Re = 9500$.

captured. The mechanism of unsteady separation and the interaction between vortical structures and solid boundary were reviewed by Doligaski *et al*. [27]. In Figure 19, the C_d values are compared with other calculated results [17, 25, 26], which show a very good agreement among the results from different methods. For the same time t, 350 000 discrete vortex elements have been used in the study of Koumoutsakos and Leonard [17] and 2044×254 grid points was used by Anderson and Reider [26]. Therefore, for high Reynolds numbers, a highly accurate solution can be obtained without using excessively large number of control vortex cells by using the finite volume method.

6. CONCLUSIONS

In this paper, we have presented a new method based on the vorticity formulation for the incompressible unsteady viscous flow. In this method, both the velocity and pressure are solved in integral formulations concerning the vorticity. The integral formulations are obtained from two Poisson equations for the velocity and pressure, respectively. The integral forms make the calculation necessary only for the flow field with no negligible vorticity and the fast summation algorithm makes the integral forms practically feasible in computing complex problems. The integral formulation for the velocity also connects vorticity boundary conditions with the instantaneous vorticity and velocity distribution in the flow domain and makes it easy to deal with the global vorticity constraints for vorticity boundary condition.

The finite volume method has been used to solve the vorticity transport equation. Inherent conservative property of the finite volume method guarantees the conservation of vorticity in the entire flow domain. The convection and diffusion of the vorticity are solved with an explicit second-order approach and an implicit Crank–Nicolson approach, respectively, and they are combined with a standard fractional step method. The scheme is simple and accurate in dealing with the vorticity boundary condition in Neumann-type. In order to accurately calculate the vorticity flux, an iterative scheme has been introduced in solving the vorticity diffusion equation.

We have demonstrated the performance of our proposed algorithm through the numerical examples. The Blasius boundary layer has been computed by time marching to a steady state after first impulsively moving the fluid in an initially zero vorticity field and the calculated results have excellent agreements with the Blasius similarity solution. Early stage development of flow around an impulsively started circular cylinder at two high Reynolds numbers has also been studied and compared with other numerical results. A higher accurate solution has been obtained without using excessively large number of grid points.

ACKNOWLEDGEMENTS

We would like to thank the reviewers for their constructive comments and suggestions.

REFERENCES

1. Batcher GR. *An Introduction to Fluid Dynamics*. Cambridge University Press: Cambridge, UK, 1967.
2. Gatski TB. Review of incompressible fluid flow computations using the vorticity–velocity formulation. *Applied Numerical Mathematics* 1991; **7**:227–239.
3. Gresho RM. Incompressible fluid dynamics: some fundamental issues. *Annual Review of Fluid Mechanics* 1991; **23**:413–453.
4. Gatski TB, Grosch CE, Rose ME. The numerical solution of the Navier–Stokes equations for three-dimensional, unsteady, incompressible flows by compact schemes. *Journal of Computational Physics* 1989; **82**:289–329.
5. Bertagnolio F, Daube O. Solution of the div-curl problem in generalized curvilinear coordinates. *Journal of Computational Physics* 1997; **138**:121–152.
6. Dennis DCR, Quartapelle L. Some of Green's theorem in solving the Navier–Stokes equations. *International Journal for Numerical Methods in Fluids* 1989; **9**:871–890.
7. Wu XH, Wu JZ, Wu JM. Effective vorticity–velocity formulation for 3D incompressible viscous flows. *Journal of Computational Physics* 1995; **122**:68–82.
8. Trujillo JT, Kaniadakis GE. A penalty method for the vorticity–velocity formulation. *Journal of Computational Physics* 1997; **149**:32–58.
9. Meitz HL, Fasel HF. A compact-difference scheme for the Navier–Stokes equations in vorticity–velocity formulation. *Journal of Computational Physics* 2000; **157**:371–403.

10. Wu JC, Thompson JF. Numerical solution of time-dependent incompressible Navier–Stokes equations using an integro-differential formulation. *Computers and Fluids* 1973; **1**:197–215.
11. Kinney PB, Paolino MA. Flow transient near the leading edge of a flat plate moving through a viscous fluid. *ASME Journal of Applied Mechanics* 1974; **41**(4):912–924.
12. Chorin AJ. Numerical study of slightly viscous flow. *Journal of Fluid Mechanics* 1973; **57**:785–796.
13. Ingbar MS, Kempka SN. A Galerkin implementation of the generalized Helmholtz decomposition for vorticity formulation. *Journal of Computational Physics* 2001; **169**:215–237.
14. Leonard A. Vortex methods for flow simulation. *Journal of Computational Physics* 1980; **37**:289–335.
15. Leonard A. Computing three-dimensional incompressible flows with vortex elements. *Annual Review of Fluid Mechanics* 1985; **17**:523–549.
16. Sarpkaya T. Computational methods with vortices—the 1988 freeman scholar lecture. *ASME Journal of Fluids Engineering* 1989; **111**:5–52.
17. Koumoutsakos P, Leonard A. High-resolution simulations of the flow around an impulsively started cylinder using vortex methods. *Journal of Fluid Mechanics* 1995; **296**:1–38.
18. Zhu B, Kamemoto K. A Lagrangian vortex method for flows over a moving bluff body. *Computational Fluid Dynamics Journal* **11**(4):363–370.
19. Cottet GH, Ould Salihi ML, Hamraoui MEI. Multi-purpose regridding in vortex methods. *ESAIM Proceedings* 1999; 94–103.
20. Koumoutsakos P, Leonard A, Pepin F. Boundary conditions for viscous vortex methods. *Journal of Computational Physics* 1994; **113**:52–61.
21. Morino L. Helmholtz decomposition revisited: vorticity generation and trailing edge condition. Part 1: incompressible. *Journal of Computational Mechanics* 1986; **1**:65–90.
22. Barnes TF, Hut P. A hierarchical $O(N \log N)$ force calculation algorithm. *Nature* 1986; **324**:446–449.
23. Lighthill MJ. Introduction. Boundary layer theory. In *Laminar Boundary Layers*, Rosenhead (ed.). Oxford University Press: Oxford, 1963.
24. Wu JZ, Wu XH, Ma HY, Wu JM. Dynamic vorticity condition: theoretical analysis and numerical implementation. *International Journal for Numerical Methods in Fluids* 1994; **19**:905–938.
25. Qian L, Vezza M. A vorticity-based method for incompressible unsteady viscous flows. *Journal of Computational Physics* 2001; **172**:515–542.
26. Anderson CR, Reider MB. A high order explicit method for the computation of flow about a circular cylinder. *Journal of Computational Physics* 1996; **125**:207–224.
27. Doligaski TL, Smith CR, Walker JDA. Vortex interactions with walls. *Annual Review of Fluid Mechanics* 1994; **26**:576–616.

